Role of breathers in the organic spin Hall effect

C. Wang,[1] Y. Y. Miao,[2] H. Ma,[1] H. X. Li,[1] H. Q. Zhang,[1] J. F. Ren,[1] C. Timm [3,4] and G. C. Hu [1,*]

[1]*School of Physics and Electronics, Shandong Normal University, Jinan 250100, China*
[2]*School of Information Science and Engineering, Shandong Agricultural University, Taian 271018, China*
[3]*Institute of Theoretical Physics, Technische Universität Dresden, 01062 Dresden, Germany*
[4]*Würzburg-Dresden Cluster of Excellence ct.qmat, Technische Universität Dresden, 01062 Dresden, Germany*

A large and oscillating spin Hall effect (SHE) in organic polymer ladders originating from polaron transport has been proposed in a previous work [Hu *et al.*, Phys. Rev. B **106**, 144309 (2022)], where a new mechanism of skew scattering off transient deformations of organic lattices caused by electron-lattice coupling has been revealed. In order to elucidate the origin of skew scattering, we analyze the components of the lattice distortions and investigate their roles in the SHE in the framework of the Su-Schrieffer-Heeger (SSH) model and the nonadiabatic dynamics method. By introducing a damping term into Newton's equation of motion, the breathers, i.e., lattice vibrations, generated by passing polarons and fueled by excess energy ultimately provided by the electric field, and charge-induced self-trapped distortions associated with the polarons themselves, are distinguished. A significant contribution to the SHE from skew scattering off the breathers is found, where the contributed percentage is related to the interchain coupling strength. Employing spectral analysis, we find that the effect of the breathers on the oscillation behavior mainly appears at low frequencies by modifying the electron transfer between chains. Moreover, by manipulating the amplitude of the breathers using a stronger field or shorter chains, the amplitude of the SHE may be controlled and enhanced. This work deepens our understanding of the microscopic mechanism of the SHE in organic polymers, and sheds light on the importance of spin-orbit physics in organic materials in spite of the weak atomic spin-orbit coupling.

I. INTRODUCTION

The spin Hall effect (SHE) [1–5] and its Onsager inverse, the inverse spin Hall effect (ISHE) [6–8], have attracted enormous interest in spintronics. The SHE realizes charge-spin conversion in an electric way, where a pure spin current is generated perpendicular to the charge current in the presence of spin-orbit coupling (SOC). In the past decades, the SHE has been widely investigated in metals [9,10] and semiconductors [11,12]. Usually, the SHE relies on intrinsic and extrinsic mechanisms [4,5]. The intrinsic mechanism is determined by the SOC of the pristine system [5], while the extrinsic mechanisms involve asymmetric scattering of spin-resolved electrons off impurities or lattice defects, where the skew-scattering mechanism [4,5,13,14] and the side-jump mechanism [4,5] are distinguished. Phonon-induced skew scattering and the resulting enhancement of the SHE was also reported for metals [15,16]. The search for the SHE in novel materials with new mechanisms is an interesting and enduring topic in spintronics.

Organic spintronics [17–20], which explores the application of electron spin in organic materials, has grown into an intriguing field due to its merits in the synthesis of low-cost and flexible devices. The pursuit of the SHE in organics is particularly attractive, but also challenging due

to the weak atomic SOC in most organic molecules. Nevertheless, there are several experimental works on the ISHE in organics, such as the spin-charge conversion in poly(3,4-ethylenedioxythiophene):poly(4-styrenesulphonate) [21,22], rubrene [23], and poly(dioctyloxy)phenylenevinylene [24]. Various ways have been attempted to achieve a sizable SHE in organics. A traditional way is to enhance the strength of the SOC, which can be achieved by doping with heavy-metal elements [25,26] or by structural conformation [27–29]. For example, the SOC strengths are 28 cm^{-1} for C atoms, but are 382 and 112 cm^{-1} for S in sixithiophene and Al in tris-(8-hydroxyquinoline) aluminum (Alq$_3$), respectively [27]. Even in metal-free molecules, the strength of the SOC can be increased by several orders of magnitude via structural modulation [27,28,30–32]. An enhanced spin-charge conversion efficiency in these systems was indeed reported [23,30].

Apart from this, exploring the role of organic intrinsic interactions in the SHE, such as the strong electron-lattice (e-l) interaction, is most important to shed light on the unique properties of the organic SHE. The strong e-l interaction makes the ground state of organic polymers dimerized, and the excitations are solitons, polarons, or bipolarons [33]. With numerical dynamical simulations, it has been demonstrated that an oscillating SHE can be realized from polaron or bipolaron transport [34–36]. An interesting result found in Ref. [34] is that the magnitude of the SHE signal from polaron transport is six orders of magnitude larger than that from electron transport in rigid chains. Therein, the enhancement of the SHE

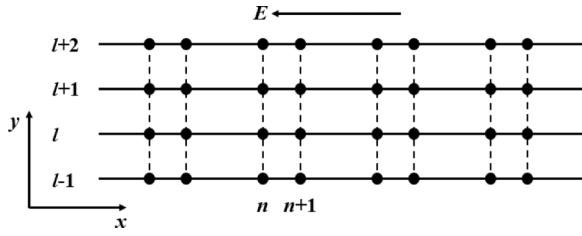---

*Contact author: hgc@sdnu.edu.cn

FIG. 1. Schematic diagram of the two-dimensional organic ladders.

is attributed to the skew scattering off transient lattice deformations generated during polaron transport. Although the phonon-induced enhancement of the SHE in metals has also been reported [15,16], the situation in organics is different and more complex. In metals, the phonons come from the lattice vibrations caused by temperature. The lattice vibrations are usually treated quantum mechanically as phonons and the electron-phonon coupling is included into the electron scattering as a self-energy term [37,38]. In contrast, in organic polymers, the lattice distortion is dominated by the Peierls dimerization in the presence of the e-l coupling. Specifically, two kinds of lattice distortion occur generically during polaron dynamics. One is the self-trapped state distortion caused by charge trapping in the presence of e-l coupling, like the usual polaron lattice distortion and other similar distortions induced by diffuse fractional charges [33,39]. The other is the breather lattice distortions left behind by the polarons. Breathers are localized distortions without charge trapping, which are generated by excess energy from the electric field after the polaron reaches a constant velocity [40]. Both kinds of lattice distortions lead to aperiodic lattice potentials and may contribute to the SHE as extrinsic scattering sources. However, the contribution of each kind to the SHE has not been identified since they appear simultaneously during polaron dynamics, making it difficult to distinguish one from the other. Extracting the effect of each kind of distortion will be helpful to understand the mechanism of organic SHE and for the design of efficient organic SHE devices.

In this work, we simulate the dynamics of polarons in coupled organic polymer chains including the SOC. By introducing a damping term into the dynamics, the amplitude of the breather lattice distortion can be modulated and even eliminated, while the polaron distortion is hardly disturbed. Thus, the role of each kind of distortion can be extracted and analyzed. The paper is organized as follows: In Sec. II, the model and methods used in this work are described. In Sec. III, the polaron dynamics are simulated and the results are discussed. A summary is given in Sec. IV.

II. MODEL AND METHODS

The model and calculation method are the same as in our previous work [34], where they are presented in detail. In the following, we will therefore keep the description brief, except where the equations are changed. We consider an anisotropic two-dimensional (2D) organic system consisting of several weakly coupled π-conjugated organic chains, aligned in the y direction as shown in Fig. 1. An electric field is applied along

the negative x direction to drive polaron transport along the organic chains. The organic lattices are described by extending the celebrated Su-Schrieffer-Heeger (SSH) model [41] by including the interchain coupling and SOC. The Hamiltonian is given as

$$H = H_e + H_{\text{latt}}. \tag{1}$$

Here, H_e is the Hamiltonian of the π electrons, including the electron hopping and the Rashba SOC. In the presence of the electric field, H_e has the form [34,35]

$$
\begin{aligned}
H_e = &-\sum_{l,n,\sigma} t_{n,n+1}^l [\exp(-i\gamma A)c_{l,n+1,\sigma}^\dagger c_{l,n,\sigma} + \text{H.c.}] \\
&- t^\perp \sum_{l,n,\sigma} (c_{l+1,n,\sigma}^\dagger c_{l,n,\sigma} + \text{H.c.}) \\
&- t_{\text{SOC}} \sum_{l,n,\sigma,\sigma'} [\exp(-i\gamma A)c_{l,n+1,\sigma'}^\dagger (i\sigma_y)_{\sigma'\sigma} c_{l,n,\sigma} + \text{H.c.}] \\
&+ t_{\text{SOC}}^\perp \sum_{l,n,\sigma,\sigma'} [c_{l+1,n,\sigma'}^\dagger (i\sigma_x)_{\sigma'\sigma} c_{l,n,\sigma} + \text{H.c.}],
\end{aligned}
\tag{2}
$$

where $t_{n,n+1}^l = t_0 - \alpha(u_{l,n+1} - u_{l,n})$ is the amplitude of intrachain hopping between sites n and $n+1$ of chain l. It is expanded in terms of the lattice distortion with t_0 being the hopping integral between two nearest-neighbor sites in a uniform chain, α the strength of the e-l interaction, and $u_{l,n}$ the displacement of site (l, n) along the x direction from its equilibrium position. $c_{l,n,\sigma}^\dagger$ and $c_{l,n,\sigma}$ are the electron creation and annihilation operators at site (l, n) with spin σ. $t^\perp$ is the interchain-hopping amplitude between two neighboring chains, which is assumed to be unchanged regardless of the $u_{l,n}$. The exponential term appears due to the electric field in the case of the periodic boundary conditions along the x direction [42]. Therein, γ is a constant used as $\gamma = ea/\hbar$, where e is the elementary charge and a is lattice constant of the organic chains in the x direction. A is the time-dependent vector potential determined by the electric field $E(t) = -\partial_t A(t)$ [43]. The intrachain and interchain SOC are represented by t_{SOC} and $t_{\text{SOC}}^\perp$, respectively, and σ_x and σ_y are Pauli matrices. Here, the possible modification to t_{SOC} by the lattice distortion is not included since t_{SOC} is small compared to the spin-independent hopping amplitude and the lattice distortion is a small quantity compared to the bond length.

H_{latt} represents the kinetic energy and elastic potential energy of the lattice,

$$H_{\text{latt}} = \frac{M}{2} \sum_{l,n} \dot{u}_{l,n}^2 + \frac{K}{2} \sum_{l,n} (u_{l,n+1} - u_{l,n})^2, \tag{3}$$

where M is the effective mass per site and K is the elastic constant.

The dynamical simulation is performed as follows. By expanding the electronic state in Wannier space, $|\Psi_\mu\rangle = \sum_{l,n,\sigma} \psi_{l,n,\sigma}^\mu |l, n, \sigma\rangle$, the ground state of the system without electric field can be calculated by solving the electronic Schrödinger equation and lattice equilibrium equation self-consistently. $\psi_{l,n,\sigma}^\mu$ is the wave function of site n with spin σ of chain l. After getting the initial state, one may simulate the time evolution of electronic states using the time-dependent

Schrödinger equation:

$$i\hbar \frac{\partial}{\partial t}\psi^{\mu}_{l,n,\sigma}$$
$$= -t^{l}_{n-1,n}\exp(-i\gamma A)\psi^{\mu}_{l,n-1,\sigma} - t^{l}_{n,n+1}\exp(i\gamma A)\psi^{\mu}_{l,n+1,\sigma}$$
$$- t^{\perp}\psi^{\mu}_{l-1,n,\sigma} - t^{\perp}\psi^{\mu}_{l+1,n,\sigma}$$
$$- t_{\mathrm{SOC}}\big[\exp(-i\gamma A)\psi^{\mu}_{l,n-1,\uparrow}\delta_{\sigma,\downarrow} - \exp(-i\gamma A)\psi^{\mu}_{l,n-1,\downarrow}\delta_{\sigma,\uparrow}$$
$$+ \exp(i\gamma A)\psi^{\mu}_{l,n+1,\downarrow}\delta_{\sigma,\uparrow} - \exp(i\gamma A)\psi^{\mu}_{l,n+1,\uparrow}\delta_{\sigma,\downarrow}\big]$$
$$+ it^{\perp}_{\mathrm{SOC}}\big[\psi^{\mu}_{l-1,n,\uparrow}\delta_{\sigma,\downarrow} + \psi^{\mu}_{l-1,n,\downarrow}\delta_{\sigma,\uparrow} - \psi^{\mu}_{l+1,n,\downarrow}\delta_{\sigma,\uparrow}$$
$$- \psi^{\mu}_{l+1,n,\uparrow}\delta_{\sigma,\downarrow}\big], \quad (4)$$

where $\delta_{\sigma\uparrow(\downarrow)} = 1$ for $\sigma =\uparrow (\downarrow)$ and 0 otherwise.

The time evolution of the lattice distortion is determined by Newton's equation of motion:

$$M\ddot{u}_{l,n}(t) = 2\alpha\mathrm{Re}\big[\exp(i\gamma A)\big(\rho^{l}_{n,n+1} - \rho^{l}_{n-1,n}\big)\big]$$
$$- K(2u_{l,n} - u_{l,n+1} - u_{l,n-1}) - \lambda M\dot{u}_{l,n}. \quad (5)$$

Here, $\rho^{l}_{n,n'}$ is the charge-density matrix defined by $\rho^{l}_{n,n'} = \rho^{l}_{n,n',\uparrow} + \rho^{l}_{n,n',\downarrow}$, where $\rho^{l}_{n,n',\sigma} = \sum_{\mu}\psi^{\mu*}_{l,n,\sigma}f_{\mu,\sigma}\psi^{\mu}_{l,n',\sigma}$. $f_{\mu,\sigma}$ is the distribution function determined by the initial occupation condition, which is 0 or 1 for each state. Unlike in our previous work [34], a damping term for the atomic motion with strength λ is included in the equation as the last term [44]. The damping term may arise from dissipation during polaron transport, which can be controlled by temperature. The purpose of introducing the damping term is to control the amplitude of the breathers. In this way, various contributions to the SHE can be distinguished, as discussed below. Equations (4) and (5) are solved by the Runge-Kutta method of order 8 with step-size control [45], which has been widely used to describe polaron dynamics [34,35,42].

The charge density and the z component of spin density are defined as

$$Q_{l,n}(t) = 1 - \rho^{l}_{n,n}(t), \quad (6)$$

$$S^{z}_{l,n}(t) = \frac{\hbar}{2}\big[\rho^{l}_{n,n,\uparrow}(t) - \rho^{l}_{n,n,\downarrow}(t)\big]. \quad (7)$$

For numerical calculations, we choose the typical values for parameters adopted popularly for polymers [33,34], $t_0 = 2.5$ eV, $\alpha = 4.1$ eV/Å, $K = 21.0$ eV/Å^2, $a = 1.22$Å, and $M = 1349.14$ eV fs^2 Å^{-2}. The interchain coupling in organic polymers is usually weak and furthermore depends on the morphology. The reasonable range used in previous studies is below 0.15 eV [46,47]. Here, we take the value as $t^{\perp} = 0.05$ eV to stabilize the polaron in the long organic ladders under investigation. The case of strong interchain coupling in some organic grids [48], where the existence of polarons is questionable, is not considered here. The strength of the SOC depends on the components and morphology of the material, as mentioned above. To make the results visible, a relatively large strength of $t_{\mathrm{SOC}} = 2t^{\perp}_{\mathrm{SOC}} = 0.02$ eV is used here, which is comparable to the one of polarons in Alq$_3$ [27]. We have also examined that the proposed physics still holds qualitatively for smaller SOC strength. The electric field is applied linearly with a turn-on time $t_c = 30$ fs, i.e., $E(t) = E_0 t/t_c$ for $0 < t < t_c$ and $E(t) = E_0$ for $t > t_c$.

III. RESULTS AND DISCUSSION

To visualize the lattice distortions generated during polaron dynamics and examine the effect of the damping term, we start from the simple case of a single organic chain consisting of 300 sites. An electron polaron is introduced centered at the 50th bond, and then an electric field of $E_0 = 1.0$ mV/Å is applied along the negative x direction. The damping term is initially turned off and other parameters are the same as mentioned above. Figure 2(a) shows the time-dependent evolution of the lattice distortion, defined as $y_n = \frac{(-1)^n}{4}(2u_n - u_{n-1} - u_{n+1})$. The clear trajectory demonstrates that the polaron moves with a saturation velocity of 0.50 Å/fs under the electric field after a short acceleration time. Since the polaron velocity as well as the kinetic energy remain unchanged, the extra energy from the driving field is absorbed by the lattice, which generates a series of breathers left behind the polaron. Figure 2(b) shows the lattice distortion and charge density at $t = 400$ fs. It is clearly seen that the lattice distortion includes the large polaron distortion induced by charge trapping and the following smaller vibrations due to breathers without any charge. The results are consistent with previous results about breathers in polymers [40].

In Figs. 2(c) and 2(d), we further show the lattice distortion and charge density in the presence of a nonzero damping term. It is found that by introducing damping, the amplitude of the breather distortions is gradually suppressed and even becomes invisible at $\lambda = 0.02$. On the other hand, the polaron distortion is hardly disturbed at $\lambda = 0.005$ and only a very slight drop of the peak is observed at $\lambda = 0.02$. Moreover, the polaron is gradually slowed down with the increase of the damping strength. This means that the proportion of breathers in the lattice distortion can be modulated efficiently by the damping term, which makes it possible to explore their role in the organic SHE.

Now, we turn to the organic ladder with transverse effects as required for the SHE. Here, three chains with 100 sites for each chain are considered, and a spin-resolved polaron initially localizes in the center of the middle chain (chain 2) is assumed. Since the interchain coupling tends to destabilize the polaron, a weak electric field of $E_0 = 0.3$ mV/Å along the negative x direction is applied to avoid the dissociation of the polaron. In the organic ladder, the lattice distortion during the polaron dynamics becomes more complicated and irregular than for the single chain due to interchain charge transfer. However, as shown in Figs. 3(a)–3(c), the two kinds of distortions mentioned above are still observed, especially in the middle chain. The breathers also exist in chains 1 and 3 but the amplitude is much smaller because of the small transferred charges ($\sim 0.15\,e$) in the case of weak interchain coupling. At strong damping of $\lambda = 0.03$, only the polaron distortions are left, including a large distortion in chain 2 and slight lattice fluctuations in chains 1 and 3. Note that although we only show the dynamics over 1400 fs in order to present a clear picture, the long-time evolution up to 6000 fs has also been examined. We observe stable polaron dynamics, also in the presence of nonzero damping or weaker interchain couplings.

To numerically evaluate the degree of lattice distortion under different damping strengths, we define the following distortion parameter to denote the deviation of lattice
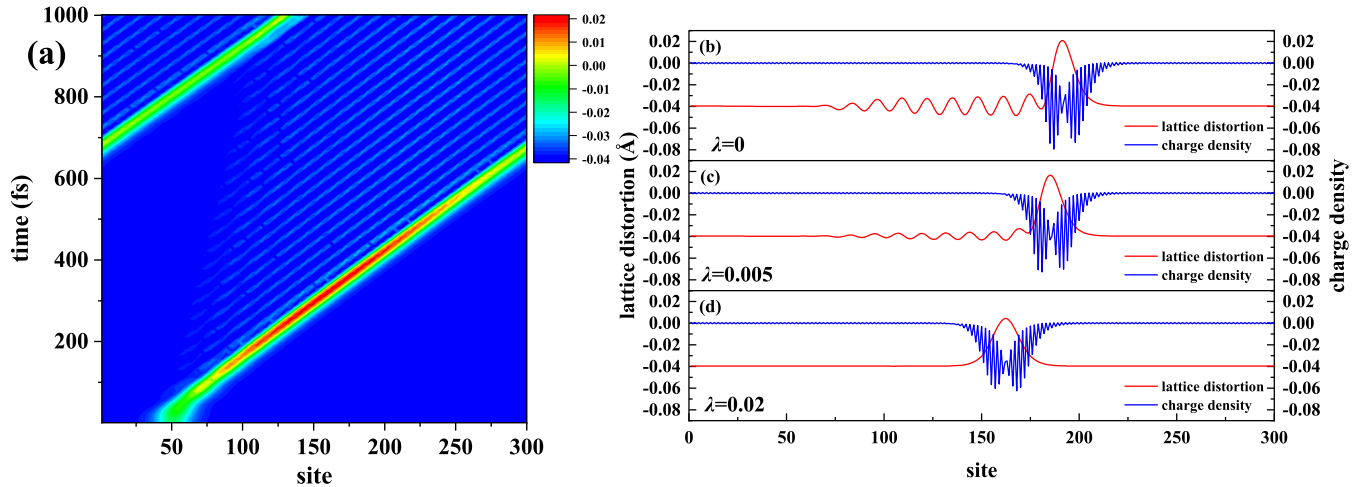
FIG. 2. (a) Time-dependent lattice distortion during polaron dynamics in a single organic chain. (b)–(d) Instantaneous lattice distortion and charge density at $t = 400$ fs with different damping parameters: $\lambda = 0$, 0.005, and 0.02, respectively.

configuration from the periodic dimerized state as

$$\sigma(t) = \sqrt{\frac{1}{3N} \sum_{l,n} [y_{l,n}(t) - y_d]^2}. \qquad (8)$$

Here, N is the number of sites per chain and y_d is the lattice distortion due to dimerization in the ground state without electron doping (~ 0.04 Å). Since the time-dependent evolution of the lattice configuration is not uniform, especially during the initial acceleration process, we use the average of σ_t over 1400 fs labeled as $\bar{\sigma}$ to determine the degree of distortion for each value of λ, where the motion of the polaron has been stable for a long time. Figure 3(d) gives the dependence of $\bar{\sigma}$ on the damping strength. It can be seen that $\bar{\sigma}$ decreases quickly from around 5.5 (in units of 10^{-3}Å here and in the following) when λ increases from zero and then changes slowly as λ becomes larger than 0.02. This is because for λ larger than 0.02 the breathers are almost completely eliminated and the lattice distortion mainly consists of the polaron distortion. We also notice an unexpected small increase of $\bar{\sigma}$ as λ changes from zero to 0.001. By checking the time-dependent lattice distortion, we find that it is caused by a somewhat larger polaron distortion although the breathers are still suppressed slightly. The reason is that the slight suppression of the breathers weakens the disturbance of the polaron distortion by the breathers.

The spin dynamics of the polaron with and without breathers are compared in Fig. 4, where the damping term is taken as $\lambda = 0$ and 0.03, respectively. We take the spin-up polaron as an example. It is found that the wavelength of the spin precession of the polaron along the chain is suppressed by the damping term, due to the lower polaron speed [42]. Moreover, the spin transfer from the central chain to the edge chains becomes much smaller at a stronger $\lambda = 0.03$. This is because the amplitude of breathers is large if the damping is very weak or absent, leading to stronger scattering of polarons and to a more irregular lattice configuration, as shown in Fig. 3(a). As a result, the binding ability of the polaron to the electron is weakened and spin transfer between chains becomes easier.

In the following, we focus on the change of the SHE with the damping term. The typical situation for the SHE is modeled through a statistical average of the time-dependent evolution of polarons with opposite spin [34]. In Fig. 5, we present the averaged total spins in each chain for various damping strengths. It is found that the oscillating SHE is robust in all cases. However, the amplitude of the averaged spins obviously decreases with increasing damping strength, where the maximum value falls to about one-half as λ increases from 0 to 0.003, and to one-quarter at $\lambda = 0.02$. However, when λ increases further to 0.03, the amplitude of the SHE changes little compared to $\lambda = 0.02$.

To understand the role of breathers in the SHE, let us recall the analysis of the mechanism for the organic SHE from polaron transport in Ref. [34]. Relative to the fast electronic-hopping processes, the lattice distortion is quasistatic and acts as a scattering potential for the electrons, which embodies in the inhomogeneity of the intrachain hopping $t_{n,n+1}^l$. Such scattering of electrons by non-SO distortion may generate two possible mechanisms for the SHE: skew scattering and side-jump scattering [5]. Reference [34] demonstrated that the SHE is proportional to the transport lifetime τ of the electrons by exploring the dependence of the SHE on the e-l coupling α, which proves that the dominated mechanism is skew scattering rather than side-jump scattering. In skew scattering, the scattering amplitude is proportional to the gradient of the aperiodic potential [2,5]. In metals, the aperiodic potential usually comes from extrinsic impurities, lattice defects, or lattice vibrations. On the other hand, in organics the aperiodic potential is related to the lattice distortion y_n, consisting of polaron and breather contributions. As shown above, the amplitude of the breather distortions is suppressed by the damping term, which decreases the gradient of lattice potential in the breathers region and thus weakens the corresponding skew scattering. If the damping term is larger enough ($\lambda > 0.02$) the breathers are almost eliminated according to Fig. 3(d). Then, the SHE is mainly contributed by the polaron distortion and is almost independent of the damping term.

In Fig. 6, the dependence of the amplitude of the SHE on the damping strength is analyzed further. For the
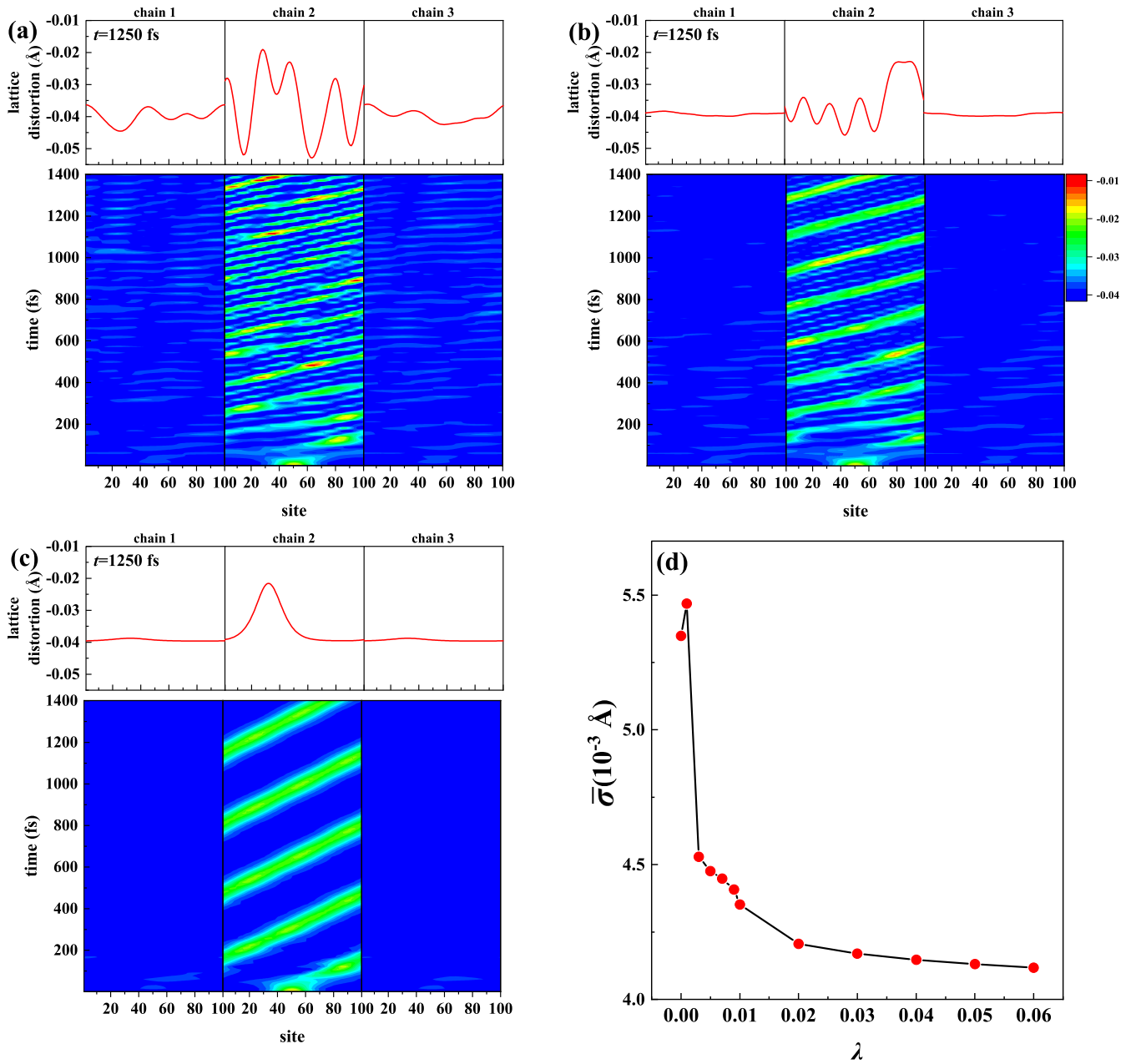
FIG. 3. (a) Time evolution of the lattice distortion and instantaneous lattice distortion at 1250 fs for the polaron dynamics in the 2D organic lattice with (a) $\lambda = 0$, (b) $\lambda = 0.003$, and (c) $\lambda = 0.03$. (d) Dependence of the averaged lattice distortion for different damping strengths.

oscillating SHE, the amplitude of the SHE is defined as the averaged magnitude of the net spins in chain 1 averaged over 1400 fs. It is found that the amplitude drops sharply when λ increases from 0 to 0.01 and then decreases slowly with increasing λ. This trend is consistent with the evolution of the degree of distortion in Fig. 3(d). To clarify the weight in the SHE induced by the breathers, we also calculate the percentage of the SHE amplitude compared with the one without the damping term. We find that at $\lambda = 0.02$, where the breathers are almost invisible, the amplitude becomes 27% of the one without the damping term. Hence, the breathers contribute 73% to the SHE in the present case.

We also note that the appearance of the damping term not only suppresses the breathers but also reduces the velocity

of the polaron, as can be seen from Figs. 3 and 4. However, the polaron velocity does not play a significant role for the SHE since the electronic-hopping process between chains is fast and the lattice deformation can be treated as quasistatic. The relevance of the polaron velocity can also be excluded based on the numerical results in Figs. 3(d) and 6. We have calculated the polaron velocities at $\lambda = 0$ and $\lambda = 0.003$, specifically, the average velocity over 1400 fs, which are 1.02 and 0.70 Å/fs, respectively. The difference between the two velocities is about 31%. At the same time, the averaged lattice distortion, shown in Fig. 3(d), decreases from 5.5 to 4.5. As a result, the amplitude of the SHE drops by 53%, as shown in Fig. 6. On the other hand, we find that when λ further changes from 0.03 to 0.06, the polaron velocity keeps decreasing from 0.36 to 0.22 fs/Å with a same drop of 31%, while the
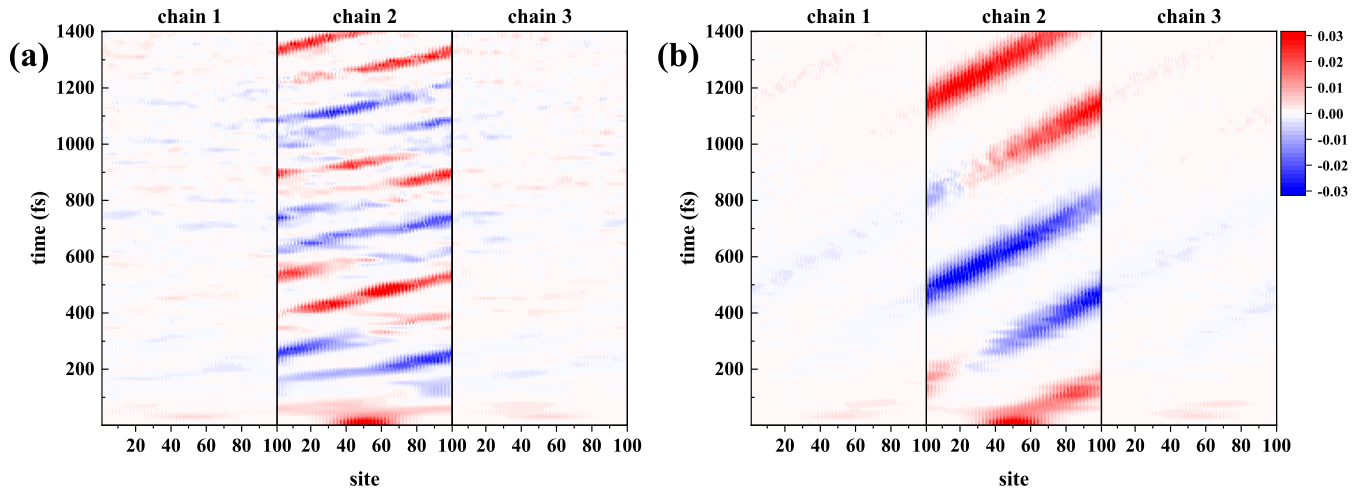
FIG. 4. Time evolution of the spin density of the spin-up polaron with and without the damping term: (a) $\lambda = 0$ and (b) $\lambda = 0.03$.

change of the degree of lattice distortion is tiny, as plotted in Fig. 3(d). We find that the amplitude of the SHE only decreases by 9%.

The effect of the damping term on the oscillation behavior of the SHE is further investigated by spectral analysis. Figure 7 shows the fast Fourier transform (FFT) of the averaged total spin in chain 1 at $\lambda = 0$, 0.003, 0.02, and 0.03. There are three characteristic frequency branches in all cases: two low-frequency parts around 0.01 and 0.03 fs^{-1} and a high-frequency part from 0.25 to 0.5 fs^{-1}. The three parts were analyzed in detail in our previous work [34], where the lowest-frequency part L1 was found to be related to the intrinsic electron transfer between chains, the middle part L2 to the appearance of polarons (e-l interaction), and the high-frequency

part H to the pure spin-flip dynamics between the chains due to SOC. It is found that the two low-frequency parts are suppressed by the damping term, especially the lowest one, while the high-frequency part is hardly disturbed. The reason is that the suppression of the breathers caused by the damping term weakens the lattice vibrations, which enhances the binding ability of the lattice to the charge and impedes the electron transfer between chains; see Fig. 8(a). To some extent, this mechanism acts like a stronger e-l interaction, which affects the two low-frequency branches in the same way, as analyzed in Ref. [34]. Note that the electron transfer between chains may also affect the SHE, similarly to the effect of $t^{\perp}$ discussed in Ref. [34]. But, here this is not the dominant reason for the change of the SHE under the damping term, as we discuss in the following.

The interchain coupling strength $t^{\perp}$ depends on the specific morphology of the organics in experiments. This parameter is crucial for charge transfer between chains, which will further affect the charge distribution and the induced lattice distortion
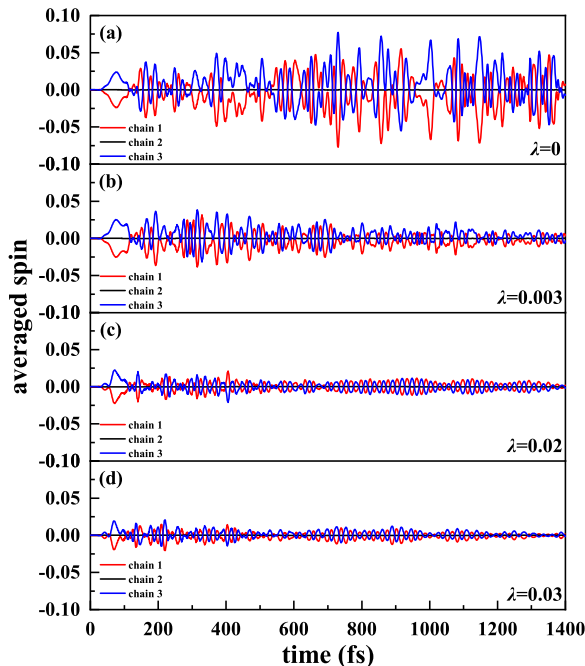

FIG. 5. The averaged spin in each chain under different damping strength: (a) $\lambda = 0$, (b) $\lambda = 0.003$, (c) $\lambda = 0.02$, and (d) $\lambda = 0.03$.
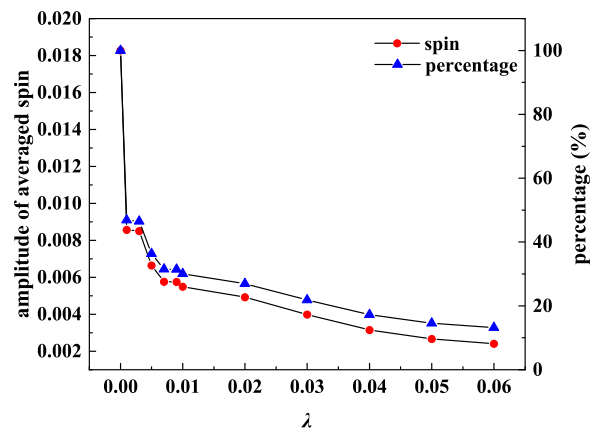

FIG. 6. The amplitude of the averaged spin (red dots) in chain 1 as a function of damping strength and the corresponding percentage (blue triangles) compared with the magnitude without damping. Here, the amplitude of averaged spin is calculated as an average over 1400 fs.
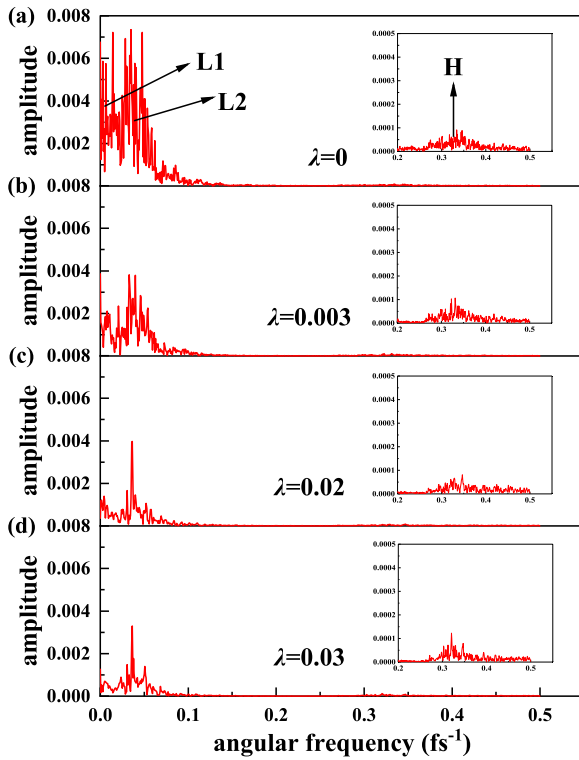
FIG. 7. Fast Fourier transform analysis of the averaged spin in chain 1 for different damping strengths: (a) $\lambda = 0$, (b) $\lambda = 0.003$, (c) $\lambda = 0.02$, and (d) $\lambda = 0.03$. The inset shows the amplitude in the frequency range of 0.2–0.5. The arrows indicate the position of three characteristic peaks: two low-frequency ones (L1, L2) and a high-frequency one (H).
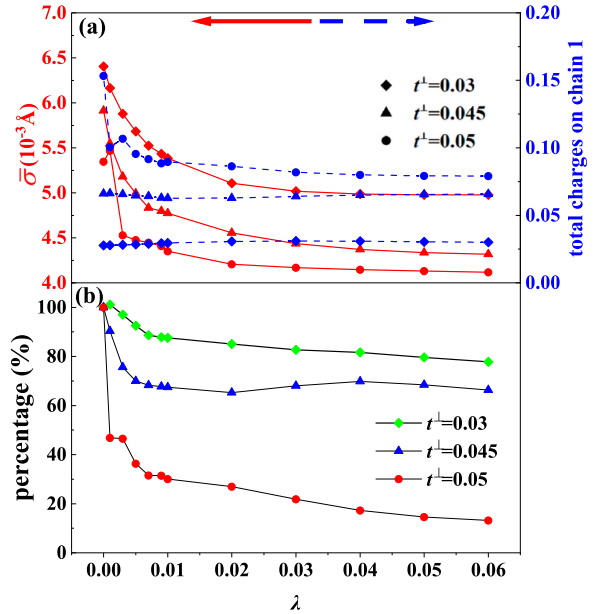

FIG. 8. (a) Lattice distortion and total charge in chain 1 as functions of the damping term for various interchain coupling strengths. (b) Percentage of the SHE amplitude defined as in Fig. 6.

in each chain. In Fig. 8, the effect of the damping term is shown for various interchain coupling strengths. In order to stabilize the polaron in the long ladders under investigation, especially in the absence of damping, we choose the interchain coupling strength to be smaller than 0.05 eV. Note that a stronger interchain coupling is permitted in the presence of damping and for shorter coupled regions. As shown in Fig. 8(a), we find that the total transferred charge in chain 1, which is the sum of charge density for all sites in chain 1 averaged over 1400 fs, is sensitive to $t^\perp$. At a stronger coupling of 0.05 eV, the total charge in chain 1 reach 0.15 without the damping term, and decreases quickly as λ grows to 0.01. For stronger damping, the total charge decreases slowly and tends to a constant of 0.08 for λ larger than 0.04. When the interchain coupling is reduced to 0.045 and 0.03, the damping term hardly affects the charge transfer due to the weak coupling strength, where the transferred charge is 0.07 and 0.03, respectively. Unlike the charge transfer, the degree of lattice distortion shows a similar dependence on the damping strength regardless of the interchain coupling strength. $\bar{\sigma}$ drops quickly as λ increases to 0.02 and then changes slowly. We also found that $\bar{\sigma}$ is a little larger for weaker interchain coupling, regardless of the strength of λ. This is because the charge transfer between chains is smaller for the weaker interchain coupling. As a result, the polaron distortion in the central chain is more pronounced and leads to a somewhat larger $\bar{\sigma}$.

Figure 8(b) shows the relative change of the SHE amplitude with λ for each interchain coupling. Obviously, the evolution of the SHE matches the change of $\bar{\sigma}$ in each case, where an apparent drop occurs when λ approaches 0.02 regardless of the interchain coupling strength. This indicates the robustness of the effect of the breathers in the organic SHE. However, we find that the contribution of the breathers differs in different situations. The decrease of the SHE for λ from 0 to 0.02 is about 73% at $t^\perp = 0.05$ eV, while the value is 35 and 15% at $t^\perp = 0.045$ and 0.03 eV, respectively. Thus, the change of the SHE induced by the breathers is also nonlinear in the interchain coupling strength. The reason is that if the interchain coupling strength is very small the charge transfer between the chains is tiny. The polaron distortion is then relatively large, which corresponds to a large effective polaron mass. In the stationary state, the polarons thus carry a large portion of the energy provided by the electric field. As a result, the amplitude of the breathers as well as their effect on the SHE is insignificant. However, if the interchain coupling is increased to 0.05 eV the charge transfer is strongly enhanced, as shown in Fig. 8(a) for $\lambda = 0$. The charge in the central chain then decreases. This leads to a decrease of the polaron distortion and, conversely, to an increase of the amplitude of breathers. In such a situation, the contribution to the SHE from the breathers becomes important. However, it should be mentioned that a large interchain coupling also destabilizes the polarons.

Finally, based on the important role of breathers in the organic SHE, it is possible to design efficient organic SHE devices by modulating the amplitude of the breathers. For example, it has been known that the amplitude of breathers relies on the strength of electric field and the chain length [40,49]. This is because a stronger field supplies more excess energy, which will increase the amplitude of breathers. In contrast, for a longer organic chain, the excess energy is distributed over
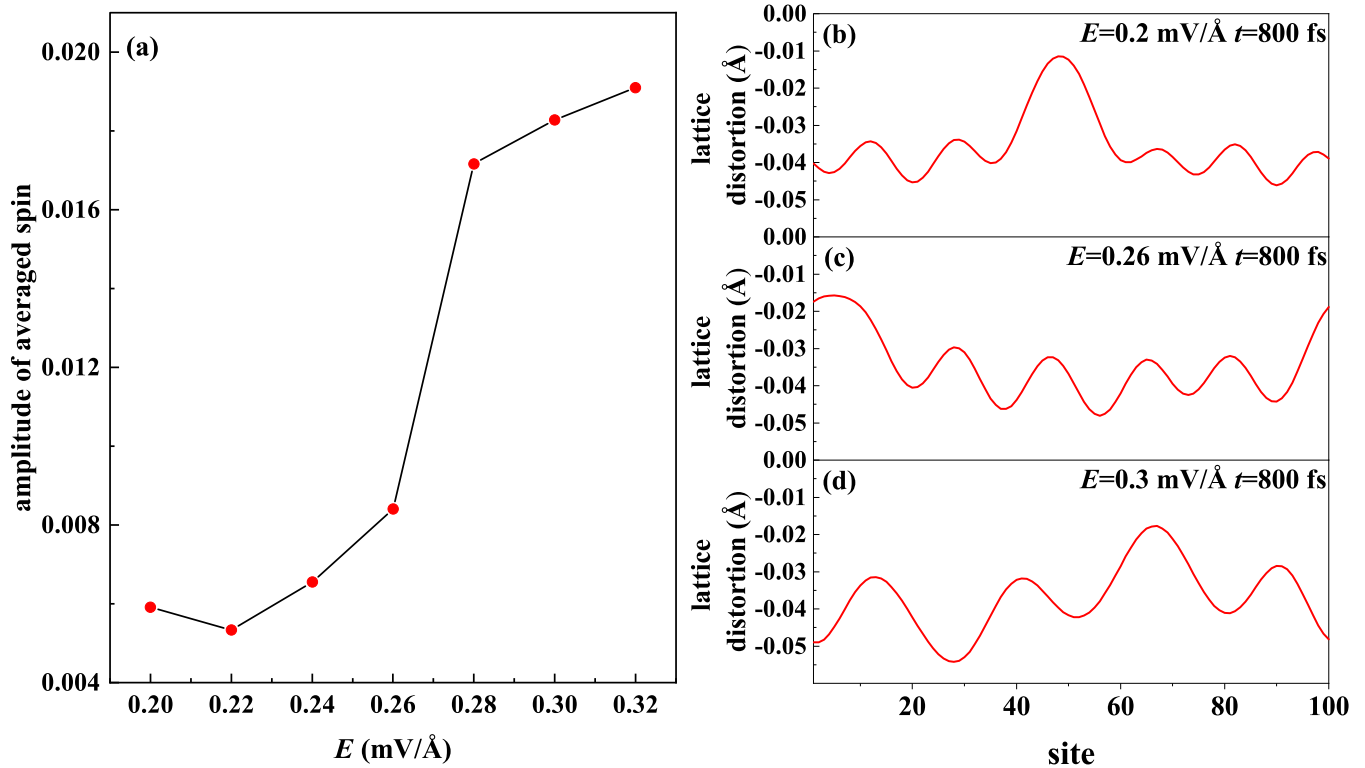
FIG. 9. (a) Averaged spin in chain 1 for different strengths of the electric field. (b)–(d) Lattice distortion in chain 2 at 800 fs for three field strengths: $E = 0.2$, 0.26, and 0.3 mV/Å.

more atoms, leading to a reduced amplitude of breathers. Such effects have been observed in soliton dynamics [49]. In Fig. 9, we first investigate the SHE and the corresponding lattice distortion for different field strengths. We find that when the field changes from 0.20 to 0.32 mV/Å, the amplitude of the SHE is enhanced by a factor of 2.5. Figures 9(b) to 9(d) show the lattice distortion of chain 2 for 0.2, 0.26, and 0.3 mV/Å, respectively. An obvious enhancement of the amplitude of breathers is seen. Fields beyond 0.32 mV/Å are not considered here since the polaron will dissociate and the physics will thus be completely different.

Figure 10 shows the time-dependent averaged spin in each chain for chain lengths $N = 100$, 150, and 200. Figures 10(a) to 10(c) demonstrate that the amplitude of the averaged spin becomes smaller in the longer chains, where the average amplitude for $N = 100$ is about 4 times larger than the one for $N = 200$. The decrease of the SHE amplitude from $N = 100$ to 150 is more distinct than the decrease from 150 to 200. This is reasonable because the change of the shared energy per site becomes smaller for increasing number of sites, and so does the amplitude of breathers. In order to check this point, the degree of lattice distortion in each case is calculated and given in Fig. 10; it is 5.35, 4.62, and 3.86, respectively. The pictures of breathers in chain 2 for each chain length are shown in Figs. 10(d) to 10(f), where the decay of the amplitude with chain length is clearly seen. Hence, a shorter chain length, which of course should be longer than the width of polarons, leads to a larger amplitude of breathers as well as to a stronger SHE.

Finally, we would like to discuss possible experimental implementations of our results. Based on the model of organic ladders, two-dimensional organic films will be ideal platforms. In experiment, the realization of two-dimensional or quasi-two-dimensional organic polymers has been reported, for example aligned polyacetylene [50,51] and polyaramid [52] films. The damping effect can be examined by modulating the dissipation via the temperature. The breathers can be probed by infrared spectroscopy to measure the lattice distortion, or by sub-5-fs pulse lasers for the breather absorption peaks [53,54]. By measuring the change of the SHE, the proposed mechanism can be verified. For three-dimensional organic materials, especially with heterogeneous structure, the intricate transport pathways and the variation of the lattice distortion between different regions would be challenging to model. It is not clear to what extent the physics we discuss survives for heterogeneous structures. However, we note that in quadrilateral prism-shaped nanotubes, the oscillating SHE from polaron transport is still observed [55]. Thus, there is hope to observe the proposed physics even in three-dimensional organic materials.

IV. SUMMARY AND CONCLUSIONS

In conclusion, the role of breathers in organic SHE has been investigated in the framework of the SSH model and nonadiabatic dynamics. By introducing a damping term into Newton's equation of motion and defining a measure of the lattice distortion, uncharged breathers and charge-induced self-trapped distortions associated with the polarons are distinguished. The results demonstrate that by increasing the damping strength, the amplitude of breathers is suppressed and can even vanish completely. At the same time, the SHE of
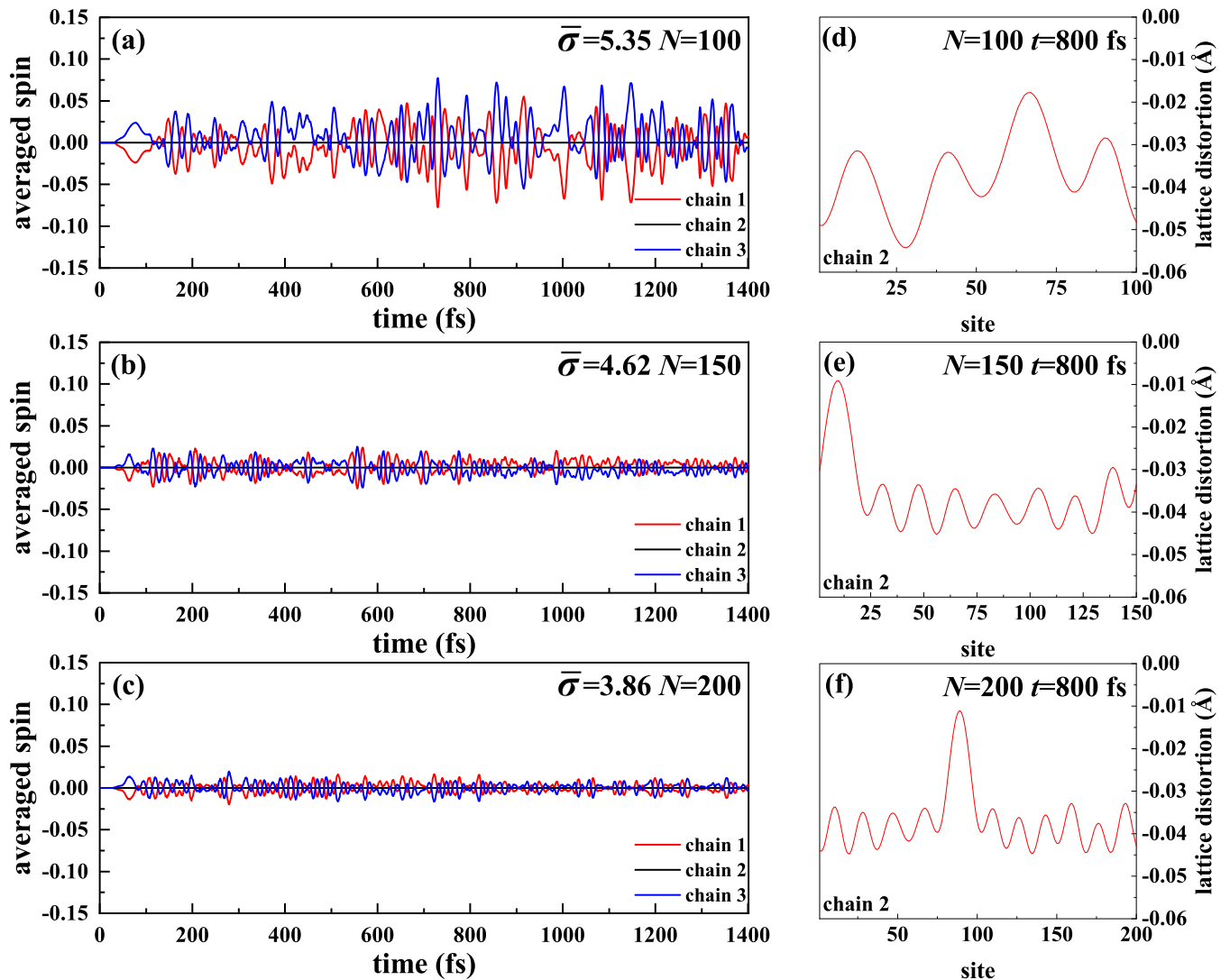
FIG. 10. Averaged spin in each chain for various chain lengths: (a) $N = 100$, (b) $N = 150$, and (c) $N = 200$. (d)–(f) Corresponding lattice distortion in chain 2 at 800 fs.

the organic chains is significantly weakened, which demonstrates a large contribution from the breathers. The role of breathers in the SHE is explained from the skew scattering off the quasistatic lattice distortion, which is reduced by the suppression of the breathers. We have also found that the contribution of the breathers to the SHE depends on the interchain coupling strength between organic chains. The reason is that a stronger interchain coupling enhances the charge transfer between chains, which reduces the charges in the central chain and thus the distortion of the polaron. Conversely, the relative amplitude of the breathers and their contribution to the SHE increase.

Applying FFT to the spin signal, we have performed a spectral analysis of the effect of damping on the oscillation behavior of the SHE. We have found that the two low-frequency parts, which originate from the intrinsic electron transfer between chains and the appearance of polarons, respectively, are suppressed by the damping term, while the high-frequency part caused by the spin-flip dynamics is hardly disturbed. This is because the suppression of the breathers caused by damp-

ing enhances the polaron distortion and thereby the binding ability of the lattice to the charge, which acts like a stronger e-l interaction and impedes the electron transfer between chains.

Furthermore, we propose that the amplitude of the SHE in organic devices can be enhanced by increasing the amplitude of breathers, e.g., applying a stronger field or using shorter chains. The former provides more excess energy to the lattice and the latter increases the energy density per site. This work deepens our understanding of the microscopic mechanism of the SHE in organic polymers, that is, the source of skew scattering off lattice distortions. It also reveals the merits of organic strong e-l interaction in the SHE, which sheds light on the spin-orbit physics in organics in spite of the weak atomic SOC.

[1] M. I. Dyakonov and V. I. Perel, JETP Lett. **13**, 467 (1971).

[2] J. E. Hirsch, Phys. Rev. Lett. **83**, 1834 (1999).

[3] S. F. Zhang, Phys. Rev. Lett. **85**, 393 (2000).

[4] G. Vignale, J. Supercond., Nov. Magn. **23**, 3 (2010).

[5] J. Sinova, S. O. Valenzuela, J. Wunderlich, C. H. Back, and T. Jungwirth, and, Rev. Mod. Phys. **87**, 1213 (2015).

[6] K. Ando, S. Takahashi, J. Ieda, Y. Kajiwara, H. Nakayama, T. Yoshino, K. Harii, Y. Fujikawa, M. Matsuo, S. Maekawa, and E. Saitoh, J. Appl. Phys. **109**, 103913 (2011).

[7] B. F. Miao, S. Y. Huang, D. Qu, and C. L. Chien, Phys. Rev. Lett. **111**, 066602 (2013).

[8] E. Saitoh, M. Ueda, H. Miyajima, and G. Tatara, Appl. Phys. Lett. **88**, 182509 (2006).

[9] A. Fert and P. M. Levy, Phys. Rev. Lett. **106**, 157208 (2011).

[10] Y. X. Ou, S. J. Shi, D. C. Ralph, and R. A. Buhrman, Phys. Rev. B **93**, 220405(R) (2016).

[11] J. Wunderlich, B. Kaestner, J. Sinova, and T. Jungwirth, Phys. Rev. Lett. **94**, 047204 (2005).

[12] M. Zarea and S. E. Ulloa, Phys. Rev. B **73**, 165306 (2006).

[13] J. Smit, Physica **21**, 877 (1955).

[14] J. Smit, Physica **24**, 39 (1958).

[15] M. Isasa, E. Villamor, L. E. Hueso, M. Gradhand, and F. Casanova, Phys. Rev. B **91**, 024402 (2015).

[16] G. V. Karnad, C. Gorini, K. Lee, T. Schulz, R. Lo Conte, A. W. J. Wells, D.-S. Han, K. Shahbazi, and J.-S. Kim, Phys. Rev. B **97**, 100405(R) (2018).

[17] V. A. Dediu, L. E. Hueso, I. Bergenti, and C. Ttaliani, Nat. Mater. **8**, 707 (2009).

[18] W. J. M. Naber, S. Faez, and W. G. van der Wiel, J. Phys. D: Appl. Phys. **40**, R205 (2007).

[19] D. L. Sun, E. Ehrenfreund, and Z. Valy Vardeny, Chem. Commun. **50**, 1781 (2014).

[20] J. S. Moodera, B. Koopmans, and P. M. Oppeneer, MRS Bull. **39**, 578 (2014).

[21] K. Ando, S. Watanabe, S. Mooser, E. Saitoh, and H. Sirringhaus, Nat. Mater. **12**, 622 (2013).

[22] M. M. Qaid, M. R. Mahani, J. Sinova, and G. Schmidt, Phys. Rev. Res. **2**, 013207 (2020).

[23] Z. H. Li, T. Li, D. C. Qi, W. Tong, L. Q. Xu, J. Zhu, Z. T. Zhang, H. Xu, W. H. Zhang, Y. X. Guo, F. Chen, Y. Y. Han, L. Cao, F. P. Zhang, and Y. M. Xiong, Appl. Phys. Lett. **115**, 053301 (2019).

[24] D. L. Sun, K. J. van Schooten, M. Kavand, H. Malissa, C. Zhang, M. Groesbeck, C. Boehme, and Z. Valy Vardeny, Nat. Mater. **15**, 863 (2016).

[25] S. Bandyopadhyay, Phys. Rev. B **81**, 153202 (2010).

[26] L. Nuccio, M. Willis, L. Schulz, S. Fratini, F. Messina, M. D'Amico, F. L. Pratt, J. S. Lord, I. McKenzie, M. Loth, B. Purushothaman, J. Anthony, M. Heeney, R. M. Wilson, I. Hernández, M. Cannas, K. Sedlak, T. Kreouzis, W. P. Gillin, C. Bernhard, and A. J. Drew, Phys. Rev. Lett. **110**, 216602 (2013).

[27] Z. G. Yu, Phys. Rev. Lett. **106**, 106602 (2011).

[28] Z. G. Yu, Phys. Rev. B **85**, 115201 (2012).

[29] S. Schott, E. R. McNellis, C. B. Nielsen, H. Y. Chen, S. Watanabe, H. Tanaka, I. McCulloch, K. Takimiya, J. Sinova, and H. Sirringhaus, Nat. Commun. **8**, 15200 (2017).

[30] M. R. Mahani, U. Chopra, and J. Sinova, arXiv:2002.11092 [cond-mat.mtrl-sci].

[31] U. Chopra, S. A. Egorov, J. Sinova, and E. R. McNellis, J. Phys. Chem. C **123**, 19112 (2019).

[32] E. Vetter, I. VonWald, S. J. Yang, L. Yan, S. Koohfar, D. Kumah, Z. G. Yu, W. You, and D. L. Sun, Phys. Rev. Mater. **4**, 085603 (2020).

[33] A. J. Heeger, S. Kivelson, J. R. Schrieffer, and W. P. Su, Rev. Mod. Phys. **60**, 781 (1988).

[34] G. C. Hu, Y. Y. Miao, and C. Timm, Phys. Rev. B **106**, 144309 (2022).

[35] Y. Y. Miao, D. Li, H. Q. Zhang, J. F. Ren, and G. C. Hu, Phys. Chem. Chem. Phys. **25**, 7763 (2023).

[36] Y. Miao, H. Zhang, H. Ma, H. Li, J. Ren, and G. Hu, Phys. Rev. B **109**, 014314 (2024).

[37] S. Tolle, C. Gorini, and U. Eckern, Phys. Rev. B **90**, 235117 (2014).

[38] C. Gorini, U. Eckern, and R. Raimondi, Phys. Rev. Lett. **115**, 076602 (2015).

[39] C. Q. Wu, Y. Qiu, Z. An, and K. Nasu, Phys. Rev. B **68**, 125416 (2003).

[40] J. F. Yu, C. Q. Wu, X. Sun, and K. Nasu, Phys. Rev. B **70**, 064303 (2004).

[41] W. P. Su, J. R. Schrieffer, and A. J. Heeger, Phys. Rev. Lett. **42**, 1698 (1979).

[42] J. Lei, H. Li, S. Yin, and S. J. Xie, J. Phys.: Condens. Matter **20**, 095201 (2008).

[43] Y. Ono and A. Terai, J. Phys. Soc. Jpn. **59**, 2893 (1990).

[44] W. Liu, K. Gao, Y. Li, Z. Sun, and D. S. Liu, Sci. China Phys. Mech. Astron. **53**, 315 (2010).

[45] R. W. Brankin, I. Gladwell, and L. F. Shampine, RKSUITE: Software for ODE IVPS, http://www.netlib.org.

[46] Å. Johansson and S. Stafström, Phys. Rev. Lett. **86**, 3602 (2001).

[47] H. A. Mizes and E. M. Conwell, Phys. Rev. Lett. **70**, 1505 (1993).

[48] H. Ozaki, M. Kasuga, T. Tsuchiya, T. Funaki, Y. Mazaki, M. Aoki, S. Masuda, and Y. Harada, J. Chem. Phys. **103**, 1226 (1995).

[49] L. M. Arancibia, C. G. Sánchez, and A. M. Lobos, Phys. Rev. B **106**, 245426 (2022).

[50] H. Shirakawa, K. Akagi, S. Katayama, K. Araya, A. Mukoh, and T. Narahara, J. Macromol. Sci.-Chem. **25**, 643 (1988).

[51] S. Y. Wang, Q. Sun, O. Gröning, R. Widmer, C. A. Pignedoli, L. L. Cai, X. Yu, B. K. Yuan, C. Li, H. X. Ju, J. F. Zhu, P. Ruffieux, R. Fasel, and W. Xu, Nat. Chem. **11**, 924 (2019).

[52] Y. W. Zeng, P. Gordiichuk, T. Ichihara, G. Zhang, E. Sandoz-Rosado, E. D. Wetzel, J. Tresback, J. Yang, D. Kozawa, Z. Y.

Yang, M. Kuehne, M. Quien, Z. Yuan, X. Gong, G. W. He, D. J. Lundberg, P. W. Liu, A. T. X. Liu, J. F. Yang, H. J. Kulik, and M. S. Strano, Nature (London) **602**, 91 (2022).

[53] S. Adachi, V. M. Kobryanskii, and T. Kobayashi, Phys. Rev. Lett. **89**, 027401 (2002).

[54] T. Kobayashi, J. Du, W. Feng, K. Yoshino, S. Tretiak, A. Saxena, and A. R. Bishop, Phys. Status Solidi C **8**, 74 (2011).

[55] L. L. Zhang, D. Pan, S. L. Zhu, and S. Q. Li, J. Phys.: Condens. Matter **35**, 255401 (2023).